Available online at www.sciencedirect.com
ScienceDirect
European Journal of Pharmaceutics and Biopharmaceutics 65 (2007) 149–162
European Journal of Pharmaceutics and Biopharmaceutics
www.elsevier.com/locate/ejpb

Research paper

Morphology of protein particles produced by spray freezing of concentrated solutions

Josh D. Engstrom [a], Dale T. Simpson [a], Edwina S. Lai [a], Robert O. Williams III [b], Keith P. Johnston [a,*]

[a] Department of Chemical Engineering, The University of Texas at Austin, Austin, TX, USA
[b] Division of Pharmaceutics, College of Pharmacy, The University of Texas at Austin, Austin, TX, USA

Received 9 March 2006; accepted in revised form 4 August 2006
Available online 18 August 2006

Abstract

The mechanisms for the formation of high surface area lysozyme particles in spray freezing processes are described as a function of spray geometry and atomization, solute concentration and the calculated cooling rate. In the spray freeze-drying (SFD) process, droplets are atomized into a gas and then freeze upon contact with a liquid cryogen. In the spray freezing into liquid (SFL) process, a solution is sprayed directly into the liquid cryogen below the gas–liquid meniscus. A wide range of feed concentrations is examined for two cryogens, liquid nitrogen (LN2) and isopentane (*i*-C5). The particle morphologies are characterized by SEM micrographs and BET measurements of specific surface area. As a result of boiling of the cryogen (Leidenfrost effect), the cooling rate for SFL into LN2 is several orders of magnitude slower than for SFL into *i*-C5 and for SFD in the case of either LN2 or *i*-C5. For 50 mg/mL concentrated feed solutions, the slower cooling of SFL into LN2 leads to a surface area of 34 m^2/g. For the other three cases with more rapid cooling rates, surface areas were greater than 100 m^2/g. The ability to adjust the cooling rate to vary the final particle surface area is beneficial for designing particles for controlled release applications.

Keywords: Spray freezing into liquid (SFL); Spray freeze-drying (SFD); Liquid cryogen; Leidenfrost effect

1. Introduction

Spray-freezing processes may be used for rapid cooling of solutions containing a therapeutic peptide or protein to produce high specific surface area (SSA) powders intended for pulmonary, transdermal, or depot delivery routes [1]. In some cases loss in protein activity in spray freezing processes has been a significant limitation [1–3]. In the spray freeze-drying (SFD) process, an aqueous solution containing dissolved protein and excipients is atomized into the cold gas above a cryogenic liquid (Fig. 1) [4–8]. The micron-sized droplets travel through the cryogenic gas, where they may begin to freeze [9], and are then completely frozen after contact with the liquid cryogen. The frozen droplets are then lyophilized leaving behind dry particles of protein and excipients. The SSA of SFD powders increases with an increase in cooling rate produced by a decrease in the aqueous droplet size [1,6,10]. High SSA particles are of practical interest as they may be micronized into sub-micron particles for uniform encapsulation into bioerodible polymer microspheres for controlled release [6,11,12].

The atomization step in SFD in the ambient gas creates a large gas–liquid interfacial area for protein adsorption and unfolding [8]. In addition, the rapid cooling of the liquid droplets produces a large ice–liquid interface which may also denature proteins [6,13]. For the protein recombinant human interferon-γ (rhIFN-γ), Webb et al. [8] demonstrated

* Corresponding author. Department of Chemical Engineering, University of Texas at Austin, 1 University Station C0400, Austin, TX 78712 1074, USA. Tel.: +1 512 471 4617; fax: +1 512 475 7824.
E-mail address: kpj@che.utexas.edu (K.P. Johnston).

0939-6411/$ - see front matter © 2006 Elsevier B.V. All rights reserved.
doi:10.1016/j.ejpb.2006.08.005

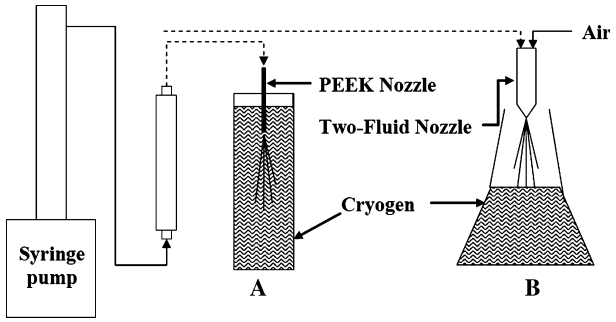

Fig. 1. Experimental apparatus for SFL (A) and SFD (B) sprays. For SFL the nozzle is immersed below the cryogen surface while for SFD the liquid jet is atomized above the liquid cryogen surface with a two-fluid nozzle.

that the gas–liquid interface is more damaging than the ice–liquid interface. Their calculations showed that a protein in the freeze concentrate during rapid cooling would not have sufficient time to diffuse to the ice–liquid interface and denature before being trapped in an amorphous glass [8]. To minimize the area of the gas–liquid interface in the SFD process the atomized droplet size may be increased, but at the expense of the SSA of the powder [1,6].

In the alternative spray freezing into liquid (SFL) process, the feed nozzle is immersed under the cryogen surface. Freezing occurs upon impingement of the feed solution with the cryogenic liquid (Fig. 1) [14]. The SFL process has been used in freezing dilute organic solutions of poorly water soluble drugs [15–18] to produce powders with high SSA and thus enhanced dissolution rates. It has also been used to spray aqueous peptide and protein solutions to achieve powders with SSA values greater than 100 m^2/g [17,19–21]. Lysozyme was shown to be more stable when produced by SFL versus SFD as a result of reduced denaturation in the spray freezing step. The improvement in stability resulted from reduced exposure to the gas–liquid interface [20].

Both the SFL and SFD processes have used liquid nitrogen (LN2) nearly exclusively as the cryogen [1–8,11,14–17,19–22]. The boiling point of LN2 is low, only −196 °C, which is desirable for rapid cooling. It is environmentally friendly, nonflammable and it does not remain as a residue in the product [18]. In spite of its low boiling point, LN2 has been shown to produce slower cooling rates than cryogens with higher freezing points such as isopentane (*i*-C5) (fp = −160 °C) and propane (C3) (fp = −190 °C) [23,24]. The lower LN2 cooling rate is well known to result from boiling of the LN2 around an inserted object, or sprayed fluid, forming an insulating gas, a phenomenon referred to as the Leidenfrost effect [23]. The influence of the Leidenfrost effect on cooling rates in SFD and SFL and on jet breakup in SFL has received little attention. Furthermore, relatively few spray freezing studies have investigated feed solutions with concentrations greater than 5 mg/mL. Scanning electron microscopy (SEM) micrographs of trehalose and sucrose powders prepared from 20% (w/v) solutions by SFD into liquid propane (SFD-C3) and into LN2 (SFD-LN2) showed very slight differences in powder morphology [25] indicating that the cooling rates in each cryogen may have been similar; however, SSA data were not available to confirm this result [25].

For SFL of dilute polyethylene glycol (PEG) solutions into liquid CO_2 at −50 °C [26] vaporization of the pressurized CO_2 was not possible and the liquid–liquid impingement readily broke up the jet into droplets [27]. For proteins including BSA and lysozyme, powders with SSAs on the order of 134 m^2/g have been produced for the SFL-LN2 process for dilute feed concentrations up to 5 mg/mL [11,21]. However, for PEG solutions, increasing the feed concentration increased the solution viscosity and inhibited liquid jet breakup resulting in slower cooling rates and larger particle sizes and eventually fibers [26]. In addition, the SSA decreases with an increase in the volume fraction of solute in the feed solution, and hence in the frozen solution [26].

The objectives of this study were to investigate morphologies (SEMs and SSAs) of protein particles, produced by both SFL and SFD into *i*-C5 and LN2 for dilute and concentrated feed solutions, in terms of jet break up, cooling rates, and nucleation and growth mechanisms. An important objective was to determine if cooling rates may be slowed down by the formation of a Leidenfrost insulating gas layer and how this influences particle morphology. Alternatively, in order to minimize solvent evaporation and to increase jet atomization, the cryogen isopentane (*i*-C5) was chosen for its low melting temperature of −160 °C, high thermal conductivity and viscosity, and high heat of vaporization and boiling point of 27 °C [23]. The differences in spray geometry and thus cooling rates will be shown to influence the SSA of the product, particularly for more concentrated solutions. Previous work with SFL in a Dewer flask with metal walls did not provide flow visualization of the jet and the frozen particles [20]. In this work, flow visualization experiments are used to show that a low viscosity turbulent gaseous N_2 cone about the sprayed jet reduces the degree of jet atomization and consequently the SSA. Thus, the SSA may be tuned by varying the cooling rate. A better mechanistic description of cooling rate and particle formation in the SFL and SFD processes will be useful for further understanding stabilities of protein powders in previous SFL and SFD studies and in a companion study of lactate dehydrogenase [28].

2. Materials and methods

2.1. Materials

Trehalose and lysozyme were purchased from Sigma Chemical Company (St. Louis, MO) and isopentane (*i*-C5) (>99% Purity) from GFS Chemicals (Powell, OH). The water was deionized by flowing distilled water through a series of 2 × 7 L mixed bed DI vessels (Water and Power Technologies, Salt Lake City, UT) containing 60:40 anionic:cationic resin blends.

2.2. Freeze procedures

2.2.1. SFL sprays

2.2.1.1. SFL into liquid nitrogen (SFL-LN2). The SFL process was modified slightly from a previous study [19]. The liquid flow rate was 10 mL/min resulting in a pressure drop of 17.2 MPa through a 63 μm ID poly-ether-ether-ketone (PEEK) nozzle 5 cm in length (Upchurch Scientific, Oak Harbor, WA) (Fig. 1). A 2 L Erlenmeyer flask containing a 2.54 cm length, 0.952 cm diameter octagonal magnetic stir bar (Fisher Scientific, Somerville, NJ) was filled with LN2 and placed in a 4 L insulated bucket (Fisher Scientific, Somerville, NJ) also filled with LN2. The ice bucket was placed on a stir plate. The depth of the LN2 vortex was approximately 2.5 cm and the nozzle was placed 2.5 cm beneath the minimum LN2 vortex level. Once the spray was completed, stirring was stopped allowing the frozen slurry to settle. Excess LN2 was decanted, and the slurry was then transferred to a 250 mL glass beaker using a spatula pre-cooled in LN2. The beakers were held in a −80 °C freezer to remove residual LN2 before transfer to the pre-cooled lyophilizer shelf.

2.2.1.2. SFL into isopentane (SFL-i-C5). The spray apparatus was based on the SFL-LN2 process, except that it was contained in a vacuum hood with care taken to eliminate all ignition sources (Fig. 1). The *i*-C5 was cooled to 4 °C in an ice–water bath. A 400 mL Pyrex® beaker was filled with 300 mL of the chilled *i*-C5, corresponding to a height of 8 cm. A smaller volume of *i*-C5 was used relative to LN2 since *i*-C5 losses due to boiling were minimal compared to LN2 during the spray. The beaker filled with *i*-C5 was placed in a LN2 bath contained in the above 4 L bucket with an inside diameter of 15 cm. The *i*-C5 was further cooled under vigorous stirring with a 2.54 cm length, 0.952 cm diameter octagonal magnetic stir bar (Fisher Scientific, Somerville, NJ). The surface of the *i*-C5 was 1.5 cm below the surface of the LN2 in the ice bucket. With a Type K thermocouple (Eutech Instruments, Vernon Hills, IL) it was found that the temperature of the *i*-C5 varied 5 °C from the center to the side of the beaker. It varied less than 1 °C as the thermocouple was positioned at different points between the top surface of the *i*-C5 in the beaker and the bottom. When the temperature in the center of the beaker reached −155 °C, the nozzle was immersed 1 cm below the cryogen surface. Solid *i*-C5 coated the inside of the beaker before and during the spray. The temperature varied less than 5 °C during the spray, as only 10–20 mL of aqueous solution was sprayed into the large thermal mass of *i*-C5.

In order to minimize the amount of *i*-C5 placed in the lyophilizer the excess *i*-C5 was filtered. An Edwards RV8 Dual-Mode Vacuum Pump (Scientific Instrument Services, Inc., Ringoes, NJ) was connected to a 1000 mL Pyrex® filtering flask (Fisher Scientific, Somerville, NJ) fitted with a porcelain Büchner funnel (Coors®, Fisher Scientific, Somerville, NJ) with an inside diameter of 11.4 cm and a circular cellulose fiber filter with a diameter of 11 cm and 1–5 μm pores (Fisher Scientific, Somerville, NJ). When the spray was complete, the ice crystal suspension in *i*-C5 was filtered for 30 s, after which the ice crystals with residual *i*-C5 were rapidly transferred to a 250 mL Pyrex® beaker filled with LN2 using a pre-cooled spatula. The residual *i*-C5 on the ice crystals was evaporated from the beakers on a lyophilizer shelf held at −60 °C under vacuum for 2 h with a LN2 trap. At −60 °C, liquid *i*-C5 has a vapor pressure of 1.08 kPa, far above a value of only 1.11 Pa for ice. The heat of vaporization of the *i*-C5 cooled the frozen slurry. Completion of the *i*-C5 evaporation was recognized by a sharp drop in the vacuum chamber pressure.

2.2.2. SFD sprays into liquid nitrogen (SFD-LN2) and isopentane (SFD-i-C5)

The SFL apparatus described above was modified for SFD (Fig. 1). The aqueous feed solution was sprayed with a 0.7 mm diameter two-fluid nozzle (Büchi, Laboratory-Techniques, Switzerland) at a constant flow rate of 10 mL/min resulting in a pressure drop of 0.827 MPa (Fig. 1). Droplet sizes were tuned by varying the air flow rates. Droplet size distributions were measured by laser light scattering (Malvern Mastersizer-S, Malvern Instruments, Ltd., Worcestershire, UK) (Fig. 2) by mounting the nozzle 10 cm above the laser beam ($\lambda = 633$ nm) and spraying the droplets normal to the laser beam. A 300 mm lens (PN 33544/777, Malvern Instruments, Ltd., Worcestershire, UK) was mounted to the detector and the sprayed droplets entered the laser beam 10–12 cm in front of the lens. Care was taken to minimize stray light entering the chamber with the laser beam. Obscuration values were between 8% and 12%.

The SFD setup was comparable to that of Maa et al. [4], who used a flow rate of 15 mL/min, and droplet sizes were similar (Table 1). The SFD nozzle was mounted 10 cm above the surface of the cryogen. Cryogen preparation and post-spray slurry collection were performed as presented in the SFL spray section, with the exception that 1 L of LN2 was utilized in a 2 L Erlenmeyer flask and 300 mL of *i*-C5 in a 1 L flask. A greater amount of LN2 was required to compensate for the 200 mL loss of LN2 after a 20 mL

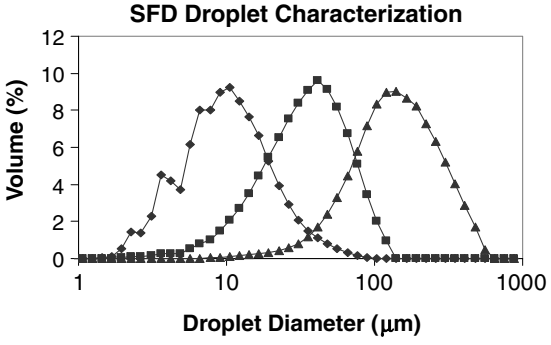

Fig. 2. Water droplets formed by SFD nozzle were measured by laser light scattering with the Malvern Mastersizer for a constant water flow rate at 10 mL/min and air flow rates at ♦ 250, ■ 150, and ▲ 50 mL/s.

Table 1
Droplet diameters formed from SFD sprays

SFD air flow rate (mL/s)	SFD liquid flow rate (mL/min)	$D(v,50)$ (μm)	Span[a]
250	10	9	2.4
290[b]	15[b]	7[b]	1.4[b]
150	10	37	2.0
167[b]	15[b]	19[b]	1.6[b]
50	10	129	2.0

[a] Span calculated as $(D_{90} - D_{10})/D_{50}$.
[b] Values from Maa et al. [3,4].

spray, due to excessive boiling whereas the losses for *i*-C5 were minimal. For SFD air flow rates of 250 mL/s, the LN2 splashed around violently inside the Erlenmeyer flask which quickly dropped the gas temperature surrounding the air plume to −196 °C, 10 cm above the cryogen surface. Reducing the air flow rates to 50 mL/s decreased LN2 splashing and increased the gas temperature to −140 °C. For no air flow, the gas temperature above the LN2 was −30 °C. For the *i*-C5 spray, the temperature of the *i*-C5 gas at a position 5 cm above the cryogen surface was −90 °C. The nomenclature for the spray configurations is as follows: spray technique-cryogen-*D(v,50)* (e.g. SFD-LN2-10 refers to the SFD configuration, with LN2 as the cryogen, and an air-flow rate that gives a droplet size $D(v,50) = 10$ μm).

2.2.3. Falling droplets into liquid nitrogen (falling droplet-LN2) and isopentane (falling droplet-i-C5)

The aqueous feed solution was passed through a 127 μm ID, 1.59 mm OD PEEK nozzle at a flow rate of 2 mL/min producing 3.6 mm diameter droplets. The nozzle was held 10 cm above a beaker of the stirred cryogen.

2.3. Drying and shelf loading

A Virtis Advantage Lyophilizer (The Virtis Company, Inc., Gardiner, NY) was used to dry the frozen slurries. The beakers containing the frozen slurries were covered with a single layer Kim-wipe held in place by a rubber-band in order to prevent powder from leaving the vial. Primary drying was carried out at −40 °C for 36 h at 300 mTorr and secondary drying at 25 °C for 24 h at 100 mTorr. A 12 h linear ramp of the shelf temperature from −40 °C to +25 °C was used at 100 mTorr.

2.4. Transfer and storage of dried powders

After the lyophilization cycle was complete, the lyophilizer was purged with nitrogen. The beakers were then rapidly transferred to a dry box held at 14% RH, and the powders were transferred to 20 mL scintillation vials. The vials were then covered with 24 mm Teflon® Faced Silicone septa (Wheaton, Millville, NJ) which were held in place by open-top screw cap lids (VWR Scientific Products, Austin, TX). Vials were purged with dry nitrogen for 2 min by inserting a needle from a dry nitrogen source through the septa with an additional needle for the gas effluent.

2.5. Surface area measurement

Surface areas of dried powders were measured with a Quantachrome Nova 2000 (Quantachrome Corporation, Boynton Beach, FL) BET apparatus. Dried powders were transferred to the glass BET sample cells in a dry box. Samples were then degassed under vacuum for a minimum of 12 h. The Brunauer, Emmett, and Teller (BET) equation [29] was used to fit adsorption data of nitrogen at 77 K over a relative pressure range of 0.05–0.30. The samples were measured two times.

2.6. Residual moisture content

Aliquots of methanol were dispensed through the septum of the scintillation vials to form a suspension concentration of 10–100 mg/mL. Vials were then placed in a tub sonicator (Mettler Electronics, Anaheim, CA) for 5 min at maximum power to insure complete suspension of the powder. Moisture content was measured for a 200 μL aliquot with an Aquatest 8 Karl-Fischer Titrator (Photovolt Instruments, Indianapolis, IN). The moisture values were corrected with a 200 μL methanol blank. All samples had a moisture content between 2% and 3% (w/w) after drying which compared well to the residual moisture contents of 2–7% (w/w) for BSA prepared by SFD as presented by Costantino et al. [6].

2.7. Particle size analysis

The size distribution of dried powders was measured by multiangle laser light scattering with a Malvern Mastersizer-S (Malvern Instruments, Ltd., Worcestershire, UK). A mass of 30–100 mg of powder was suspended in 10 mL of acetonitrile and the suspension was then sonicated on ice for 1 min using a Branson Sonifier 450 (Branson Ultrasonics Corporation, Danbury, CT) with a 102 converter and tip operated in pulse mode at 35 W. Typical obscuration values ranged from 11% to 13%. Aliquots of the sonicated suspension were then dispensed into a 500 mL acetonitrile bath for analysis.

2.8. Scanning electron microscopy

SEM images were collected on a Hitachi Model S-4500 scanning electron microscope (Hitachi Ltd., Tokyo, Japan). The samples were prepared in a dry-box. Aluminum stages fitted with double adhesive carbon conducting tape were gently dipped into sample vials until covered by powder. Stages were then placed in septum capped vials and purged with nitrogen for transfer. To minimize the time samples were exposed to atmospheric moisture the stages were rapidly transferred to a Pelco Model 3 sputter-coater. A conductive gold layer was applied and the

samples were then quickly transferred to the SEM. Total exposure to the atmosphere was less than 1 min.

3. Results

3.1. SFL

Solutions containing lysozyme and trehalose were sprayed at different feed concentrations into both LN2 and *i*-C5 (Table 2). For a lysozyme feed concentration of 5 mg/mL extremely high SSAs were obtained for both cryogens. The SSA for 5 mg/mL lysozyme in LN2 was comparable to previous values for SFL of bovine serum albumin (BSA) [11,20]. Concentrated lysozyme samples at 50 mg/mL and above had SSAs three to four times higher when sprayed in *i*-C5 relative to LN2. For 50 mg/mL solutions sprayed in *i*-C5, surface areas were above 100 m^2/g. To validate that the lysozyme SSA values achieved in Table 2 were not affected by moisture exposure the residual moisture contents of the dried powders of all lysozyme formulations were determined by Karl Fischer titration. For residual moisture contents up to 7–8% (w/w) the known glass transition temperature (T_g) for lysozyme is ~50 to 60 °C [30], and for lower moisture contents the T_g is expected to be higher. The low moisture contents of 2–3% (w/w) measured for all dry powder samples, as mentioned in section 2.6, shows that the drying protocol was sufficient to produce lysozyme powders with a T_g much higher than room temperature. Therefore, it was expected that loss in lysozyme powder SSA due to moisture exposure would be negligible. As a further comparison and control concentrated 50 and 100 mg/mL trehalose feed concentrations processed by SFL had SSAs nearly five times greater in *i*-C5 than in LN2. The ability to achieve high surface areas for trehalose, which is hygroscopic, suggests that our sample transfer procedures did not cause significant losses in SSA from increases in molecular diffusion due to exposure to moisture.

As the lysozyme feed concentration increased from 5 to 100 mg/mL for SFL-LN2 sprays, the submicron particle content after sonication decreased from 85% to 29% on a volume percentage basis (Table 2). The SFL-*i*-C5 submicron content remained 76% even for a high feed concentration of 100 mg/mL. Selected sonicated size distribution peaks are given in Fig. 3 and showed that the submicron $D(v,50)$ peak for all powders was approximately 0.30 μm. Similar particle sizes for sonicated BSA powder prepared by SFD-LN2 for 20 mg/mL formulations were measured by Costantino et al. [6]. However, a second peak with much larger sizes was present for the SFL-LN2 spray at 50 mg/mL (Fig. 3).

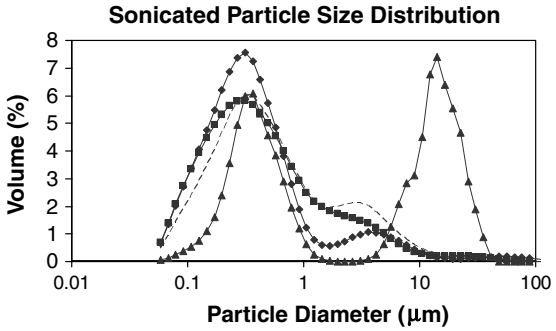

Fig. 3. Particle size distributions of lysozyme samples processed at ♦ 5 mg/mL in SFL-LN2, and 50 mg/mL in ▲ SFL-LN2, ■ SFL-*i*-C5, and – SFD-LN2-10 after sonication as measured by laser light scattering.

In SFL-LN2 (Fig. 4A) the nozzle tip was hidden by a large gaseous froth at the surface yet a narrow liquid jet was observed to penetrate at least 10 cm into the cryogen without breakup. To better visualize the ice particles a dyed solution was sprayed through the SFL nozzle. Large dyed ice crystals appeared to emanate from the bottom of the jet and subsequently were circulated in the flask by the large gas flux of evaporating LN2. Following the spray, large, dense crystals were suspended in the quiescent LN2. For the SFL-*i*-C5 spray, it was easy to observe the spray, since evaporation of cryogen was minimal. A wide jet angle was apparent at the tip of the nozzle and the jet break up length was less than 0.5 cm. The intense jet atomization lead to a fine dispersion of ice particles (Fig. 4B). After stopping the spray, the particles remained suspended for approximately 1 min.

Table 2
Specific surface area measurements and particle size distributions of lysozyme and trehalose powders processed by SFL

Component	Feed concentration (mg/mL)	SSA (m^2/g)		Size (μm)[a]	
		LN2	*i*-C5	LN2	*i*-C5
BSA[b]	5	134	–	0.050–1.0 (92%) 1.0–2.0 (8.0%)	–
Lysozyme	5	114 ± 11	164 ± 8	0.050–1.0 (85%) 2.0–10 (15%)	–
Lysozyme	50	34 ± 2	124 ± 15	0.050–1.0 (48%) 4.0–12 (52%)	0.050–1.0 (80%) 3.0–11 (20%)
Lysozyme	100	38 ± 2	111 ± 4	0.050–1.0 (29%) 6.0–40 (71%)	0.050–1.0 (76%) 3.5–11 (24%)
Trehalose	50	14 ± 2	84 ± 11	–	–
Trehalose	100	13 ± 1	70 ± 6	–	–

[a] Particle size distribution of powders measured by laser light scattering after sonication.
[b] Values from Leach et al. [11].

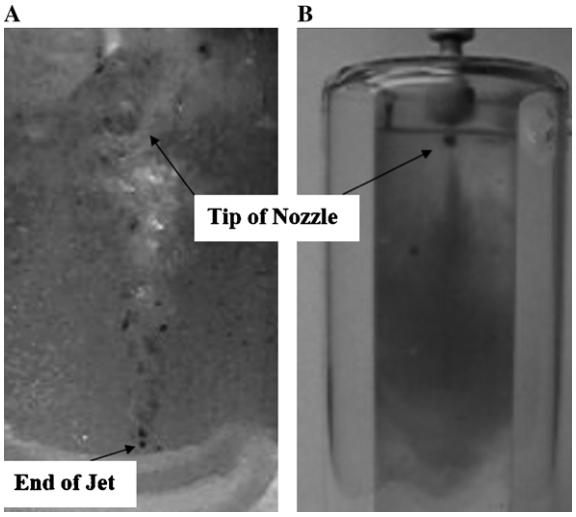

Fig. 4. SFL of dye solution sprayed at 10 mL/min as seen through a double glass dewar in LN2 (A) and *i*-C5 (B). *i*-C5 temperature is −100 °C.

Selected SEM images from the results in Table 2 are shown in Fig. 5 for the 5 and 50 mg/mL lysozyme formulations. Both the 5 mg/mL SFL-LN2 and SFL-*i*-C5 particles (Fig. 5A and B) were extremely fine showing spherical particle structures approximately 50 nm in diameter that were joined together. For 50 mg/mL SFL-LN2 (Fig. 5C), large sheets were observed with morphological features greater than 1 μm. The 50 mg/mL SFL-*i*-C5 primary particles were extremely fine, 100 nm in diameter, with necks between the aggregated primary particles (Fig. 5D). This type of morphology has been observed for SFL-LN2 sprays of 5–10 mg/mL BSA feed concentrations [11]. The calculated SSA for 100 nm diameter nonporous spheres assuming a particle density of 1 g/cm^3 is 60 m^2/g and the measured SSA for the SFL-*i*-C5 for a 50 mg/mL lysozyme feed concentration was 124 m^2/g, indicated limited internal porosity. The powder SSA for the 50 mg/mL lysozyme SFL-LN2 spray was 34 m^2/g, consistent with the much larger features in the SEM micrograph.

3.2. SFD

For 50 mg/mL lysozyme sprayed by SFD-LN2, there was a substantial decrease in SSA and decrease in the volume percentage of submicron particles for an increase in aqueous solution droplet size (Table 3). For SFD-*i*-C5 the SSA was moderately larger for 10 μm droplets relative to 40 or 130 μm droplets. The particle size distribution was similar for 10 and 130 μm droplets. For the 10 and 40 μm droplets, the SSAs and particle size distributions were similar for both cryogens. However, sprays into *i*-C5 resulted in a much larger SSA and particle size relative to LN2 for the 130 μm droplets. As mentioned for SFL, the SFD sprays follow the same pattern for volume percentage of submicron sonicated particles versus droplet size as presented by Costantino et al. [6] As shown in Fig. 3, the $D(v,50)$ for the SFD submicron peak was 0.3 mm.

SEM micrographs of SFD powder formed from 10 μm aqueous droplets frozen over *i*-C5 and LN2 had similar morphologies (Fig. 6A and B) with 100 nm diameter necks between the aggregated primary particles. These morphol-

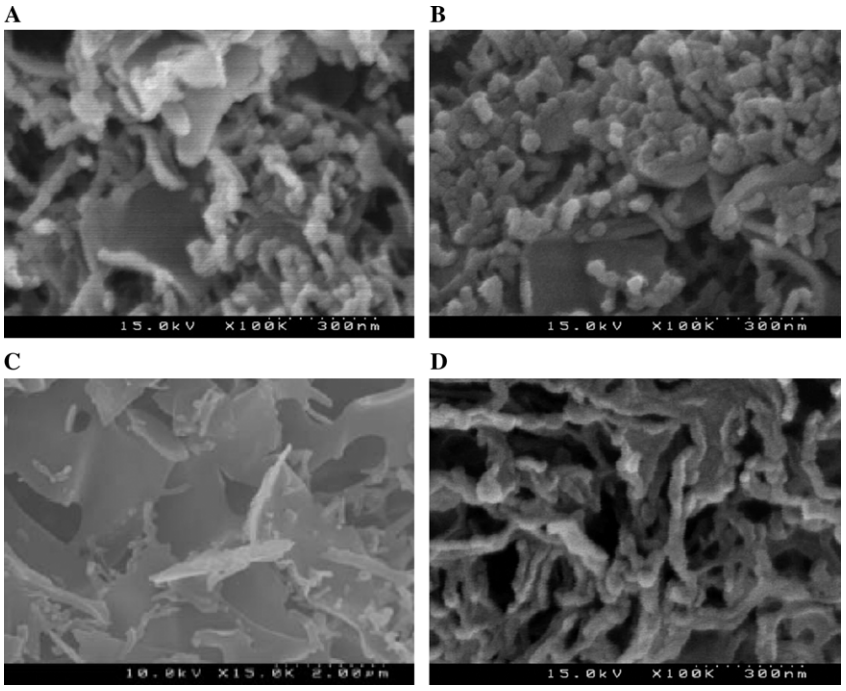

Fig. 5. SEMs of 5 mg/mL lysozyme formulations for SFL-LN2 (A), SFL-*i*-C5 (B), and 50 mg/mL lysozyme formulations for SFL-LN2 (C), and SFL-*i*-C5 (D). Liquid flow rate was 10 mL/min.

Table 3
Specific surface area measurements and particle size distributions of lysozyme powders processed by SFD and SFL

Freeze process	Droplet size (μm)	SSA (m^2/g)		Size (μm)[a]	
		LN2	*i*-C5	LN2	*i*-C5
SFD	10	126 ± 5	129 ± 2	0.050–1.0 (74%) 1.0–10 (26%)	0.050–1.0 (64%) 3.0–11 (36%)
SFD	40	87 ± 3	68 ± 2	0.050–1.0 (52%) 3.0–12 (48%)	0.050–1.0 (47%) 3.5–12 (53%)
SFD	130	26 ± 1	90 ± 2	0.050–1.0 (38%) 5.0–11 (62%)	0.050–1.0 (74%) 3.0–10 (26%)
Falling droplet	3600	4.2 ± 0.02	22 ± 0.3	0.20–1.0 (23%) 3.5–13 (77%)	0.050–2.0 (65%) 4.0–11 (35%)
SFL	–	34 ± 2	124 ± 5	0.050–1.0 (48%) 4.0–12 (52%)	0.050–1.0 (80%) 3.0–11 (20%)

Lysoyzme feed concentration was 50 mg/mL for all sprays.
[a] Particle size distribution of powders measured with a Malvern Mastersizer after sonication.

ogies resemble the 50 mg/mL SFL-*i*-C5 (Fig. 5D) lysozyme spray. For 50 mg/mL solutions, the SFL-LN2 particles (Fig. 5C) are 10 times larger compared to the particles prepared by SFD (Fig. 6A and B) or SFL with *i*-C5 (Fig. 5D). The SFD-LN2-130 (Fig. 6C) spray formed large sheets with 1 μm sized morphological features similar to the SFL-LN2 spray in Fig. 5C. The SFD-*i*-C5-130 spray had morphologies more similar to the 10 μm droplet SFD sprays with 200 nm necks between aggregated primary particles.

Additional experiments were performed with lysozyme concentrations held at 50 mg/mL, while trehalose was added to form the appropriate formulation ratios shown in Table 4. The SFD sprays were conducted at an air flow rate of 250 mL/s to form 10 μm droplets (Table 1, Fig. 2). For each lysozyme:trehalose formulation in Table 4, powder SSAs were large, above 100 m^2/g despite the high feed concentration of over 50 mg/mL. The SSA decreased modestly with increasing trehalose content. The SSAs were independent of cryogen type. The lysozyme:trehalose SSAs were compared to the rhDNase:trehalose powders presented in Maa et al. [3,4] where the same two-fluid nozzle and protein:sugar ratios were used. For high protein:trehalose ratios, the SSAs for the lysozyme:trehalose and rhDNase:trehalose formulations were both above 100 m^2/g, but the SSAs decreased well below 100 m^2/g with increasing sugar content for the rhDNase:trehalose formulations. The discrepancy may be attributed to the difference in lyophilization protocols. Maa et al. performed the primary drying step at a shelf temperature of −25 °C [4] which is

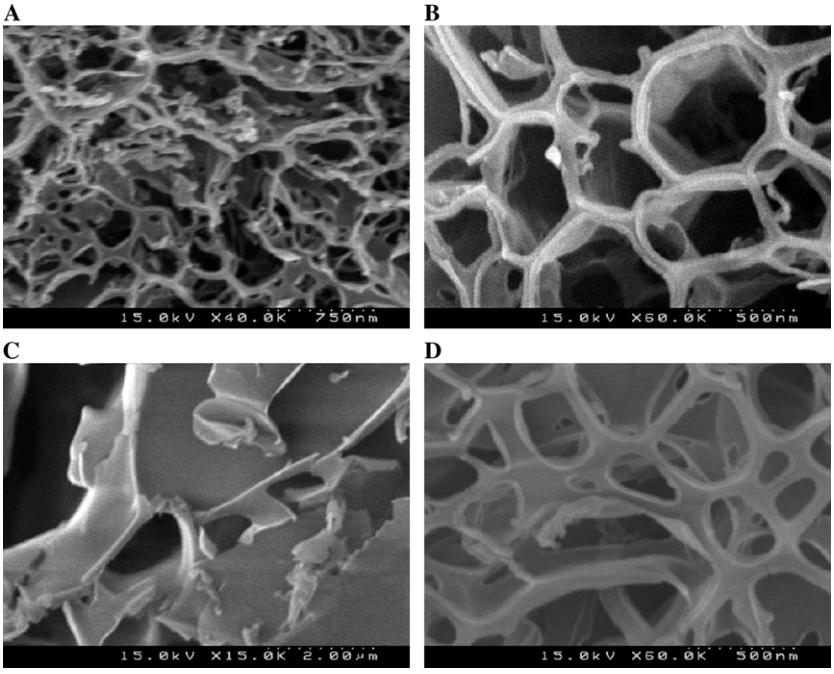

Fig. 6. SFD sprays of 50 mg/mL lysozyme formulations for 10 μm diameter droplets processed by SFD-LN2-10 (A), SFD-*i*-C5-10 (B), and for 130 μm diameter droplets processed by SFD-LN2-130 (C), SFD-*i*-C5-130 (D).

Table 4
Specific surface area measurements of protein and sugar powders processed by SFD for 10 μm diameter droplets over *i*-C5 and LN2

Loading ratio of protein:trehalose in spray formulation	SSA (m^2/g)		
	Lysozyme-*i*-C5	Lysozyme-LN2	rhDNase-LN2[a]
80:20	162 ± 4	147 ± 4	111
60:40	134 ± 3	131 ± 3	71
40:60	120 ± 2	113 ± 2	5

Lysozyme feed concentration was 50 mg/mL for all formulations.
[a] Values from Maa et al. for the protein rhDNase [3].

slightly above the measured T'_g of trehalose at −31 °C [31]. Meltback of trehalose during drying may have caused a significant decrease in powder SSA with an increase in trehalose content. In our study, the shelf temperature during primary drying was −40 °C and was sufficiently cold to prevent meltback of trehalose during drying, to preserve a high surface area.

3.3. Falling droplet

The SSA for falling droplet-*i*-C5 was approximately five times greater than for falling droplet-LN2 (Table 3). During the cooling process for falling droplet-LN2 the spherical liquid droplet impacted the LN2 and then floated on the LN2 surface due to surface tension. After approximately 30 s the boiling around the frozen droplet ceased as the droplet was fully solidified, and the droplet sank to the bottom of the beaker. During cooling in the LN2 two droplets occasionally coalesced into a larger droplet. Therefore, ice formation may not be completed for at least 30 s after the liquid droplet impacts the LN2 surface. For the falling droplet-*i*-C5 process the drop impacted the *i*-C5 surface and then immediately sank without boiling. Impaction with *i*-C5 caused the 3.6 mm diameter droplet to deform into a 4–5 mm diameter dish shape (Fig. 7). The greater deformation of the droplet is consistent with the much smaller interfacial tension between water and *i*-C5 versus water and LN2. The resulting volume percentage of submicron particles formed by falling droplet-*i*-C5 was much greater at 80% than for falling droplet-LN2 at 48%, and approached values observed for the spray freezing processes, despite lower SSAs.

4. Discussion

4.1. Jet breakup

The breakup of liquid jets has been studied for jets sprayed into a gaseous atmosphere [32,33], into liquids [34], and into supercritical fluids [27,35–38]. For liquid jets sprayed into a gas at atmospheric pressure, Rayleigh and atomization jet breakup boundaries have been characterized using the Ohnesorge number *Oh* (viscous to surface tension forces) $= \mu_j/(\rho_j D_o \sigma)^{1/2}$, and $Re_j = \rho_j U D_o/\mu_j$, where the subscript *j* stands for liquid jet and μ,ρ, D_o, and σ are the viscosity, density, jet diameter, and interfacial tension, respectively [32,33]. For jets sprayed into a quiescent gas or a liquid such as in SFL, *U* is the jet velocity whereas for the SFD sprays with a two-fluid nozzle *U* is the relative velocity of the air to the liquid jet [32]. As either *Re* and/or *Oh* increases, the liquid jet breakup mechanism crosses the boundary from the Rayleigh regime to the atomization regime [33,39]. In the Rayleigh breakup regime the droplet sizes are slightly larger than the liquid jet diameter and jet breakup occurs far downstream from exiting the nozzle. In the atomization regime, droplet diameters are an order of magnitude smaller than the jet diameter and jet breakup occurs immediately upon exiting the nozzle [33].

For sprays into gases at low pressures, typically the shear stress at the fluid interface is neglected [36]. Experimentally, it has been shown for liquid jet sprays into dense gaseous atmospheres [38] and into liquids [34], the much larger ambient values of μ_a and ρ_a facilitate jet breakup at lower *U*. The above correlation for sprays into gases is no longer valid [38,39]. The Weber number *We* (inertial to interfacial forces) $= \rho_a U^2 D_o/\sigma$ has been used for liquid jets sprayed into gases of varying density [32] and into supercritical fluids [27,35] to correlate jet breakup length. To account for the effects of ρ_a and μ_a, Czerwonatis et al., have modified the *Oh* number to form a new dimensionless number, Z^{**}, which is defined as [38]:

$$Z^{**} = Oh \cdot \sqrt{We} \cdot \sqrt{\frac{\mu_a}{\mu_j}} = \frac{\mu_j \cdot U}{\sigma} \cdot \sqrt{\frac{\rho_a}{\rho_j}} \cdot \sqrt{\frac{\mu_a}{\mu_j}} \quad (1)$$

On the basis of experiments with liquid jets in pressurized nitrogen and carbon dioxide, Rayleigh and atomization boundaries were determined and correlated in terms of Z^{**} versus Re (Fig. 8) [38].

Table 5
Calculation of Reynolds (*Re*), Weber (*We*) and Z^{**} numbers for SFL and SFD sprays

Nozzle	Ambient fluid/temperature (°C)	Air flow rate (mL/s)	*U* (m/s)	σ (mJ/m^2)	ρ_a (g/cm^3)	*We*	*Re*	Z^{**}
SFD	Air (25 °C)	250	611	74	0.0011	2.8×10^3	4.7×10^5	3.6×10^{-2}
SFD	Air (25 °C)	150	366	74	0.0011	1.0×10^3	2.8×10^5	2.1×10^{-2}
SFD	Air (25 °C)	50	122	74	0.0011	1.1×10^2	9.4×10^4	7.1×10^{-3}
SFL	*i*-C5 (−155 °C)	–	53	50	0.77	2.8×10^3	3.7×10^3	1.7
SFL	LN2 (−196 °C)	–	53	74	0.81	2.0×10^3	3.7×10^3	0.25
SFL	GN2 (−196 °C)	–	53	74	0.0044	11	3.7×10^3	3.4×10^{-3}

The property value $\mu_j = 0.91$ (mPa s) for water at 25 °C was used to calculate *Re* and Z^{**}.

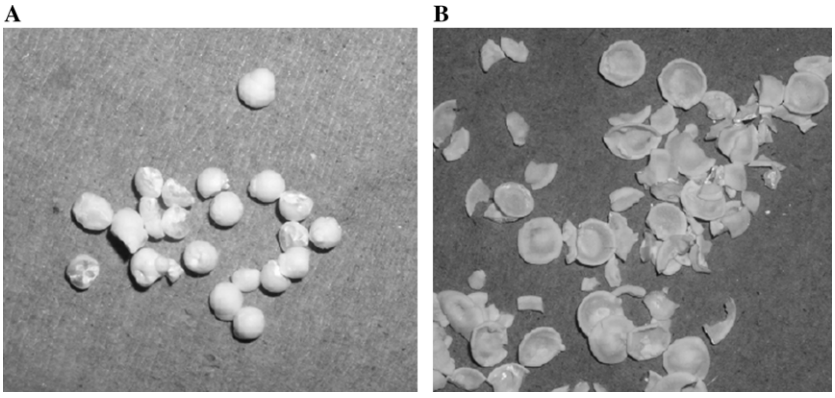

Fig. 7. Droplets frozen by the falling droplet process into LN2 (A) and *i*-C5 (B). Feed formulation was 50 mg/mL lysozyme.

In Fig. 8 it is shown that each SFD spray condition with the two-fluid nozzle was in the atomization regime. The 10, 40, and 130 μm droplets are all much smaller than the original 0.7 mm diameter nozzle for the liquid jet, which is consistent with atomization, rather than Rayleigh breakup. As shown in Fig. 8, the SFD sprays approach the atomization-transition boundary as the *Re* number decreases with a decrease in *U*. The *Re* values, based on the jet properties, were identical for the SFL sprays regardless of the cryogen since the liquid flow rate and nozzle diameter were fixed (Table 5). The SFL-*i*-C5 spray was in the atomization region in Fig. 8, consistent with the rapid jet break up in Fig. 4.

The SFL-LN2 spray formed a liquid jet ~10 cm long within an inverted gaseous cone of evaporating nitrogen as shown in Fig. 4. Therefore, two limits were considered for nitrogen at −196 °C, either gaseous or liquid conditions. The Z^{**} number calculated for gaseous properties (SFL-GN2) was in the Rayleigh regime. It was two orders of magnitude lower than the Z^{**} numbers for liquid properties (SFL-LN2), which were in the atomization regime. The spray patterns in Fig. 4 suggested that the jet did not fan out within the gaseous N_2 cone, as would have been the case for spraying into a viscous liquid. Thus, the determination of Z^{**} with gaseous properties is more indicative of the behavior in Fig. 4 than Z^{**} calculated with liquid properties. The low viscosity of the nitrogen within the cone produced by excessive boiling (Leidenfrost effect) caused the SFL spray to behave like an SFL-GN2 spray.

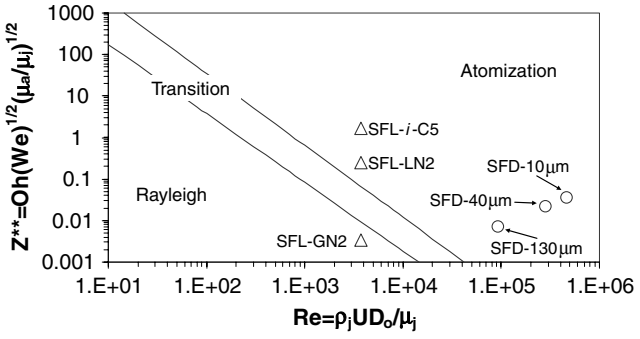

Fig. 8. Jet breakup regimes correlated with Z^{**} and *Re* for SFL sprays into *i*-C5, LN2, and GN2 and SFD sprays for 10, 40, and 130 μm diameter droplets.

It is possible that the turbulent cone consisted of gaseous voids mixed with pockets of LN2 droplets. In this case, the properties of the continuous N_2 phase would correspond to those of a mixture of liquid and gas. The very low interfacial tension of LN2 and turbulence of the boiling N_2 would facilitate mixing of the liquid and gaseous domains.

4.2. Cooling rate calculation

For SFD and SFL a forced convective heat transfer coefficient (h) was calculated with spherical droplets moving through a cryogenic medium at constant velocity. Droplet sizes were measured for SFD whereas the droplet sizes for SFL were inferred as explained below. The correlation for h is given below and is valid for gaseous or liquid flow past spheres [40,41]:

$$\frac{hD_d}{k_a} = 2 + (0.4Re_a^{0.5} + 0.06Re_a^{0.67})Pr^{0.4}\left(\frac{\mu_a}{\mu_s}\right)^{0.25} \quad (2)$$

where D_d, k_a, Pr, and μ_s are the droplet diameter, ambient thermal conductivity, Prandtl number using ambient fluid properties, and ambient viscosity corresponding to the temperature of the droplet surface, respectively. Re_a is calculated with ambient fluid properties and the velocity of the liquid droplets, U. U is the velocity of the liquid jet exiting the nozzle for SFL. For SFD, it was assumed that the atomized liquid droplets moved at the same velocity as the air. The velocity of the air stream 10 cm away from the nozzle was calculated with the continuity equation for a cone of expanding air where UA is constant.

The h was used to determine if the droplets were cooled in a convective-limited or conductive-limited regime. In the convective-limited regime the temperature gradients throughout the liquid droplet are negligible as it cools, whereas in the conductive-limited regime the temperature gradients are significant [41,42]. The cooling regime can be determined by calculating the Biot number for spheres,

$Bi = hD_d/6k_d$, which is a ratio of convective to conductive heat transfer where k_d is the droplet thermal conductivity [41,42]. In the regime where $Bi < 1$ the cooling of the droplet is convection-limited although some sources place the boundary at $Bi < 0.1$ [40–43]. In this work, both the convection-limited and conduction-limited calculations are presented when the calculated Bi number is in the range $0.1 < Bi < 1$ (Table 6). For the convection-limited regime, with no resistance in the droplet phase, the average cooling rate for the droplet at an initial temperature T_i is estimated as [42,43]:

$$\frac{dT}{dt} \approx \frac{A}{V} h(T_i - T_a) \frac{1}{\rho \cdot C_p} \quad (3)$$

where T is the droplet temperature at time t and ρ, C_p, A, and V are the droplet density, heat capacity, surface area, and volume, respectively. In the regime, where $Bi \geqslant 1$ the heat transfer mode is conduction-limited. For the cooling rate in the conduction-limited regime [42,43], with no resistance in the cryogen phase,

$$\frac{dT}{dt} \approx \left(\frac{A}{V}\right)^2 k(T_i - T_a) \frac{1}{\rho \cdot C_p} \quad (4)$$

The cooling rate calculations (Table 6) neglect the latent heat of fusion of water and assume complete vitrification of the aqueous droplets, as has been assumed previously [42,44]. Experimental studies of samples plunged into cryogens have shown that cooling rates of samples that undergo a phase change are not significantly different from those that do not [42,45]. In this work, cooling times in the convective-limited and conductive-limited regime were calculated by integrating Eqs. (3) and (4) over the temperature range from 298 to 173 K (Table 6). The lower temperature limit of 173 K was chosen for the cooling calculations (Table 6) since the major amount of ice crystallization occurs in the temperature range of 273–173 K for slow cooling [24]. Thus, it was of interest to know the cooling times for this dangerous temperature range where it is desirable to avoid ice crystallization.

As shown on Table 6 for 10 and 40 μm diameter droplets, the calculated cooling times for SFD-*i*-C5 and SFD-LN2 sprays were similar, consistent with the similar SSAs and particle morphologies (Tables 2 and 3 and Fig. 6). The Leidenfrost effect may be expected to be relatively small for the 10 μm diameter atomized droplets in SFD-LN2 because of their small diameter. The SFD droplets that were 130 μm in size produced smaller morphological features and higher SSAs in *i*-C5 verses LN2 indicating faster cooling (Fig. 6C and D) despite similar calculated cooling times. An explanation for this discrepancy is that the droplets were large enough for some evaporation of nitrogen to slow the cooling rate in LN2 versus *i*-C5 leading to a lower powder SSA. If the solutions were sprayed into gaseous N_2 at −196 °C, the calculated cooling times would be at least two orders of magnitude slower (Table 6) versus liquid N_2.

To calculate SFL cooling times, the droplet sizes in each cryogen were estimated from the images shown in Fig. 4. For SFL-*i*-C5 the cooling time was calculated for 10 μm spheres due to the intense breakup of the liquid jet from the 63 μm nozzle whereas the SFL-LN2 and SFL-GN2 cooling times were calculated for 100 μm spheres since liquid jet breakup was minimal. Calculated cooling rates for SFL-*i*-C5 sprays were the same order of magnitude as for the SFD-LN2-10 and SFD-*i*-C5-10 sprays. This result is consistent with the similar 100 nm morphological features in Fig. 5D and Fig. 6A and B. Given these similar morphologies and cooling times, it is likely that these sprays are frozen primarily by liquid–liquid contact with a minimal, if any, Leidenfrost effect for N_2.

The calculated SFL-LN2 cooling time was an order of magnitude slower than for SFL-*i*-C5, as a result of the larger droplet size. For SFL-GN2, it was three orders of magnitude slower. The resulting SFL morphology (Fig. 5C)

Table 6
Calculated Reynolds number (*Re*), Prandtl number (*Pr*), average convective heat transfer coefficient (*h*) and Biot number (*Bi*) for each spray process

Nozzle	Cryogen	Droplet diameter (μm)	*Re*	*Pr*	$h/10^4$ (W/m^2-K)	*Bi*	Cooling time (ms)	Cooling rate/10^4 (K/s)
SFD	*i*-C5	10	1.7	35	12	0.37[a]	0.014–0.038	330–890
SFD	*i*-C5	40	4.2	35	4.4	0.53[a]	0.22–0.43	29–56
SFD	*i*-C5	130	4.5	35	1.4	0.54[a]	2.4–4.4	2.9–5.3
SFD	GN2	10	6.6	0.75	0.21	0.0062[b]	1.9	6.6
SFD	GN2	40	16	0.75	0.061	0.0073[b]	26	0.49
SFD	GN2	130	17	0.75	0.019	0.0074[b]	270	0.047
SFD	LN2	10	41	2.4	12	0.36[a]	0.012-0.033	380–1100
SFD	LN2	40	97	2.4	4.4	0.53[a]	0.19–0.36	35–66
SFD	LN2	130	110	2.4	1.4	0.54[a]	2.0–3.6	3.4–6.3
SFL	*i*-C5	10	120	35	87	2.6[c]	0.014	890
SFL	GN2	100	4400	0.75	0.23	0.067[b]	17	0.72
SFL	LN2	100	27000	2.4	35	10[c]	1.2	11

[a] Cooling times and cooling rates are represented as a range where the lower limit is the convection-limited regime and the upper limit is the conduction-limited regime.
[b] For *Bi* numbers <0.1 only convection-limited cooling was calculated.
[c] For *Bi* numbers >1 only conduction-limited cooling was calculated.

and SSA (Table 2) were similar to those for the SFD-LN2-130 morphology (Fig. 6C and Table 3). Thus, it is likely that some of the nitrogen also evaporated about the 130 μm drops in SFD. As droplet sizes increased to 3.6 mm in the falling droplet experiments the same difference in powder SSA resulted from liquid-gas contact in falling droplet-LN2 versus liquid–liquid contact for falling droplet-*i*-C5.

4.3. Mechanism of vitrification of aqueous solutions

The morphology of an aqueous solution in the frozen state depends on the cooling rate [45]. Fig. 9 shows a phase diagram for sucrose, a non-crystallizing solute in water [45–48]. Protein and sugar solutions subjected to slow cooling rates on a temperature controlled shelf in a tray lyophilizer have a low degree of supercooling beneath the equilibrium freezing curve [48]. The water in the supercooled solution nucleates and forms crystalline ice [45]. The latent heat of crystallization causes the temperature of the supercooled solution to rise to the equilibrium freezing curve [45,48]. Globular proteins and most sugars remain in the unfrozen solution known as the freeze concentrate and are usually kinetically hindered from crystallizing [45]. As liquid water moves from the unfrozen phase to the ice phase during freezing, the composition of the freeze concentrate follows the equilibrium freezing curve toward T'_g, the point where the solution is maximally freeze concentrated (Fig. 9) [48]. At this point the unfrozen domains become sufficiently viscous that they vitrify [48].

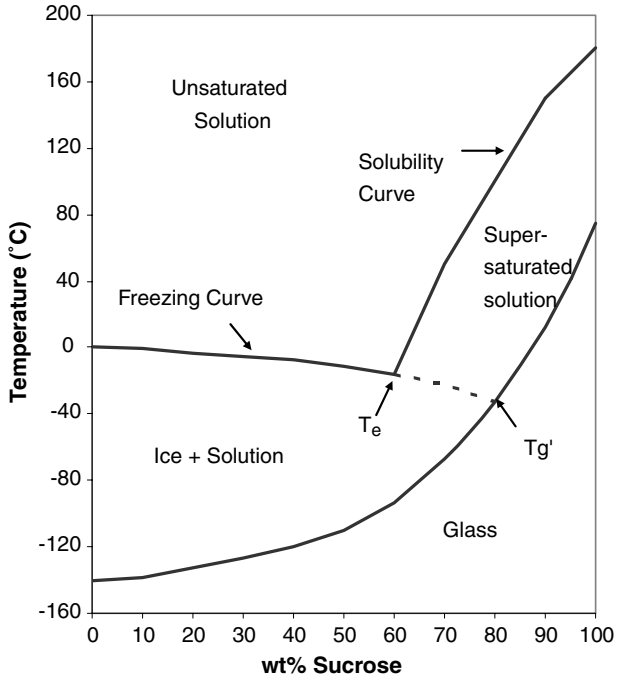

Fig. 9. Solid–liquid diagram for the sucrose-water system. Adapted from Fig. 7 of Nail et al. [48].

Ultra rapid cooling rates of aqueous solutions, for example in jet sprays, do not follow the equilibrium path as described above [45,47]. Rapid cooling minimizes the time for the formation and growth of ice crystals as the aqueous solution passes through the critical temperature zone [9,19,49], which is the region between the equilibrium freezing curve and the T_g curve where liquid water can nucleate to form crystalline ice. The temperature may pass below the T_g curve fast enough to minimize, or even fully prevent, nucleation of ice crystals [45]. Fletcher calculated that to vitrify a 1 μm diameter water droplet and prevent ice crystal formation requires a cooling rate of 10^{10} K/s [50]. The presence of sugar and/or water miscible polymers in solution can help facilitate vitrification and slow crystal growth which could decrease the cooling rate for vitrification[45]. Liquid water jets with diameters sufficiently small (~10 μm) sprayed at velocities of 250 m/s led mostly to vitrified water [51]. The cryogens were propane and ethane, to avoid the Leidenfrost effect, and the frozen water was analyzed by X-ray diffraction (XRD) [45,51].

When a supercooled aqueous solution passes through the critical temperature zone, the solute may become supersaturated from a decrease in solubility before the water vitrifies. As shown in Fig. 9, the solubility curve decreases with decreasing temperature and ends at the eutectic temperature, T_e. For temperatures well below T_e, it is not possible to measure a true equilibrium sucrose solubility in liquid water. However, for rapid non-equilibrium supercooling of the water without time to freeze, the solubility of sucrose in hypothetical supercooled liquid water would be expected to decrease with temperature. For example, the ideal solubility of a solid in a liquid decreases as the difference between the melting point of the solid and the temperature increases. Furthermore, the decrease in solubility with temperature is evident in Fig. 9 above T_e. The decrease in solubility with temperature may even lead to supersaturation and nucleation and growth of solute from the unfrozen solution even before a significant amount of vitrification of water occurs. For a liquid–liquid phase separation two glasses with two separate T_g values can be formed upon vitrification [52]. For PEG/dextran formulations used to stabilize recombinant hemoglobin, increasing the cooling rate of the formulations lead to increased stability [22]. The increased hemoglobin stability has been attributed to prevention of phase separation of the polymer, dextran and PEG, from the protein due to increased cooling rates [22].

In the SFD and SFL processes, the high degree of supercooling rapidly leads to temperatures far below the T_g curve in Fig. 9. Vitrified water domains form as relatively few water molecules have enough time to reach the crystalline state. The detailed relaxation dynamics for rapid vitrificaton of sucrose and lysozyme solutions are the subject of current study [53]. Therefore, in this study, the SEMs of the lysozyme morphology are utilized to shed insight into the vitrification mechanism during the spray freezing processes. Although changes in the morphology of the lysoyzme

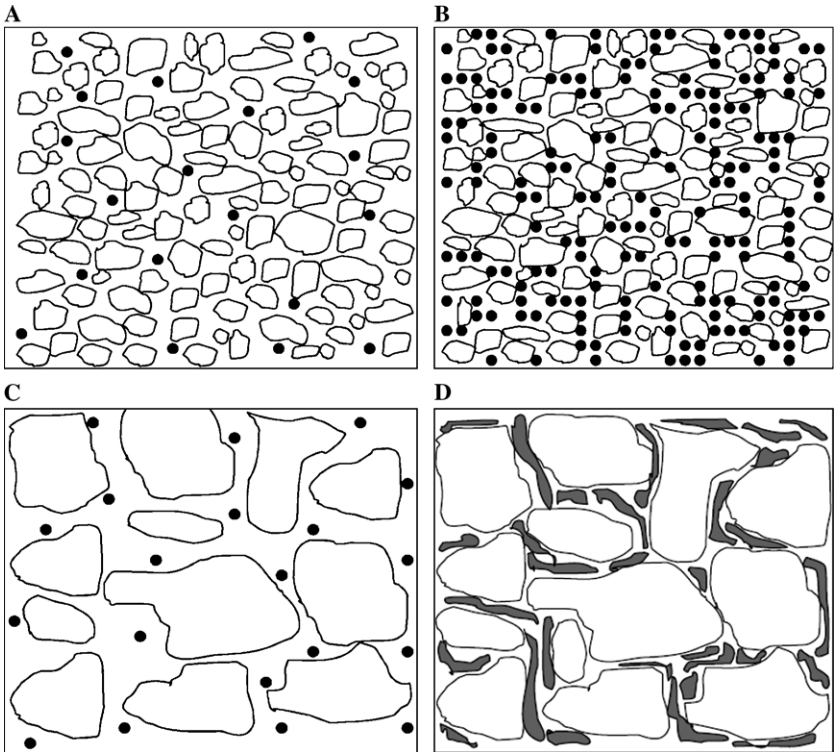

Fig. 10. Frozen morphologies of dilute solution with high supercooling (A), concentrated solution with high supercooling (B), dilute solution with low supercooling (C), and concentrated solution with low supercooling (D). Amorphous ice particles are represented as white domains and solute precipitate as solid dots or gray regions.

are possible during lyophilization, the temperature was maintained below T'_g during lyophilization to minimize such changes.

Based on the SEM results and above discussion of freezing processes, a proposed schematic of the role of solute concentration and cooling rate is presented in Fig. 10. For all of the cryogens and spray freezing processes in this study, dilute 5 mg/mL lysozyme solutions led to particles on the order of 50 nm in diameter and surface areas greater than 100 m^2/g (Table 2). As shown in Fig. 10A, for dilute aqueous solutions subjected to a high degree of supercooling, the high nucleation rates lead to small glassy domains of water and small solute domains in the unfrozen water between the finely divided glassy water domains. Between the vitrified water domains, the thin films of unfrozen water, containing solute particles, limit the collisions and hence aggregation/coalescence of the solute particles. The rapid heat transfer vitrifies all of the water quickly, limiting the time for coalescence of solute particles.

For more concentrated solutions, in this case 50 mg/mL, the lysozyme particles formed a web with 100 nm connecting necks as shown in Figs. 5D, Fig. 6A and B. In Fig. 5D which was the SFL-*i*-C5 spray for a 50 mg/mL lysozyme formulation, protein threads are formed as opposed to the more spherical protein domains as seen in Fig. 5B. Here, the larger solute concentration leads to a greater volume fraction of vitrified solute domains in the unfrozen water channels, and thus a greater collision frequency and increased aggregation/coalescence. The higher concentration also leads to more rapid transport of solute molecules to these growing domains. The result is larger and more aggregated particles after lyophilization as shown in Fig. 10B.

For dilute solutions, the morphologies were similar for the slower SFL-LN2 process and the other three more rapid spray processes. The final particle size is on the order of 100 nm. Here, the low concentration of the solute leads to a small number of growing solute particles, a low collision rate, and consequently a low aggregation rate, as shown schematically in Fig. 10C. The aggregation rates are slow despite the thick channels of unfrozen water between particles. The entire matrix becomes vitrified before significant growth of the small number of particles takes place.

For concentrated solutions, for example 50 mg/mL, subjected to slower rates of cooling in the SFL-LN2 process, as a consequence of the Leidenfrost effect, large plates of particles with significantly smaller surface areas were observed in Fig. 10D, relative to the other conditions in Fig. 10B. For a slower cooling rate, the lower degree of supercooling decreases the nucleation rate. A longer time is available for the smaller number of nucleated vitrified water domains and precipitated solute domains to grow. As shown schematically in Fig. 10D, the solute particles that nucleate and grow in the relatively large channels between vitrified water particles have significant time to coalesce and form thin plates before vitrification is complete.

5. Conclusions

The SFL and SFD spray processes were utilized to produce high surface area lysozyme particles over a wide range of feed concentrations for two cryogens, LN2 and isopentane (*i*-C5). For dilute aqueous solutions up to 5 mg/mL, the focus of most previous studies, the dried powder SSAs were $>100\ m^2/g$ in SFL for each cryogen indicating cooling was rapid enough to prevent substantial particle growth. Even for viscous feeds with concentrations as high as 100 mg/mL, powders with SSAs greater than $100\ m^2/g$ were produced in the SFD and SFL-*i*-C5 processes indicating sufficient atomization for rapid cooling and quenching relative to particle growth. For SFD with either cryogen, powder SSAs and SEMs were shown to be negligibly impacted by the droplet diameter for droplets less than 100 μm suggesting the Leidenfrost effect was unimportant. For SFL, LN2 was found to form a turbulent gaseous N_2 cone around the sprayed jet. The low viscosity gas layer reduced the degree of jet atomization for N_2, but not for the non-evaporating cryogen *i*-C5. The calculated cooling rate for SFL in LN2 was three orders of magnitude lower than in *i*-C5 or SFD with either cryogen. For 50 mg/mL concentrated feed solutions, SSAs were on the order of $34\ m^2/g$ for SFL into LN2 and the features in the SEMs were courser, consistent with the slower cooling rates. The ability to adjust the cooling rate to vary the final particle surface area will be beneficial for designing particles for controlled release applications. The high protein feed concentrations offer the potential of high production rates, as well as smaller volumes of solvent that must be sublimated in lyophilization.

Acknowledgements

This material is supported in part by the STC Program of the National Science Foundation under Agreement No. CHE987664, the Robert A. Welch Foundation, and the Separations Research Program at the University of Texas. The authors also thank Ted Randolph for highly useful suggestions in the design of this project.

References

[1] Y.-F. Maa, H.R. Costantino, Spray freeze-drying of biopharmaceuticals: applications and stability considerations, in: H.R. Costantino, M.J. Pikal (Eds.), Biotechnology: Pharmaceutical Aspects. 2. Lyophilization of Biopharmaceuticals, American Association of Pharmaceutical Scientists, Arlington, 2004, pp. 519–561.

[2] X.C. Nguyen, J.D. Herberger, P.A. Burke, Protein powders for encapsulation: a comparison of spray-freeze drying and spray drying of darbepoetin alfa, Pharm. Res. 21 (2004) 507–514.

[3] Y.-F. Maa, S.J. Prestrelski, Biopharmaceutical powders: particle formation and formulation considerations, Curr. Pharm. Biotechnol. 1 (2000) 283–302.

[4] Y.-F. Maa, P.-A. Nguyen, T. Sweeney, S.J. Shire, C.C. Hsu, Protein inhalation powders: spray drying vs spray freeze drying, Pharm. Res. 16 (1999) 249–254.

[5] Y.-F. Maa, P.-A. Nguyen, Method of spray freeze drying proteins for pharmaceutical administration, U.S. Patent, 6,284,282 (2001).

[6] H.R. Costantino, L. Firouzabadian, K. Hogeland, C.C. Wu, C. Beganski, K.G. Carrasquillo, M. Cordova, K. Griebenow, S.E. Zale, M.A. Tracy, Protein spray-freeze drying. Effect of atomization conditions on particle size and stability, Pharm. Res. 17 (2000) 1374–1383.

[7] H.R. Costantino, L. Firouzabadian, C.C. Wu, K.G. Carrasquillo, K. Griebenow, S.E. Zale, M.A. Tracy, Protein spray freeze drying. 2. Effect of formulation variables on particle size and stability, J. Pharm. Sci. 91 (2002) 388–395.

[8] S.D. Webb, S.L. Golledge, J.L. Cleland, J.F. Carpenter, T.W. Randolph, Surface adsorption of recombinant human interferon-γ in lyophilized and spray-lyophilized formulations, J. Pharm. Sci. 91 (2002) 1474–1487.

[9] Z.H. Chang, J.G. Baust, Ultra-rapid freezing by spraying/plunging: pre-cooling in the cold gaseous layer, J. Microsc. 161 (1991) 435–444.

[10] W. Wang, Lyophilization and development of solid protein pharmaceuticals, Int. J. Pharm. 203 (2000) 1–60.

[11] W.T. Leach, D.T. Simpson, T.N. Val, E.C. Anuta, Z. Yu, R.O. Williams III, K.P. Johnston, Uniform encapsulation of stable protein nanoparticles produced by spray freezing for the reduction of burst release, J. Pharm. Sci. 94 (2005) 56–69.

[12] W.T. Leach, D.T. Simpson, T.N. Val, Z. Yu, K.T. Lim, E.J. Park, R.O. Williams III, K.P. Johnston, Encapsulation of protein nanoparticles into uniform-sized microspheres formed in a spinning oil film, AAPS Pharm. Sci. Tech. 6 (2005) 605–617.

[13] B.S. Chang, B.S. Kendrick, J.F. Carpenter, Surface-induced denaturation of proteins during freezing and its inhibition by surfactants, J. Pharm. Sci. 85 (1996) 1325–1330.

[14] R.O. Williams III, K.P. Johnston, T.J. Young, T.L. Rogers, M.K. Barron, Z. Yu, J. Hu, Process for production of nanoparticles and microparticles by spray freezing into liquid, U.S. Pat. Appl. Publ. 2,004,022,861 (2004).

[15] J. Hu, T.L. Rogers, J. Brown, T. Young, K.P. Johnston, R.O. Williams III, Improvement of dissolution rates of poorly water soluble APIs using novel spray freezing into liquid technology, Pharm. Res. 19 (2002) 1278–1284.

[16] J. Hu, K.P. Johnston, R.O. Williams III, Rapid dissolving high potency danazol powders produced by spray freezing into liquid process, Int. J. Pharm. 271 (2004) 145–154.

[17] T.L. Rogers, J. Hu, Z. Yu, K.P. Johnston, R.O. Williams III, A novel particle engineering technology: spray-freezing into liquid, Int. J. Pharm. 242 (2002) 93–100.

[18] T.L. Rogers, A.C. Nelsen, J. Hu, J.N. Brown, M. Sarkari, T.J. Young, K.P. Johnston, R.O. Williams III, A novel particle engineering technology to enhance dissolution of poorly water soluble drugs: spray-freezing into liquid, Eur. J. Pharm. Biopharm. 54 (2002) 271–280.

[19] Z. Yu, T.L. Rogers, J. Hu, K.P. Johnston, R.O. Williams III, Preparation and characterization of microparticles containing peptide produced by a novel process: spray freezing into liquid, Eur. J. Pharm. Biopharm. 54 (2002) 221–228.

[20] Z. Yu, A.S. Garcia, K.P. Johnston, R.O. Williams III, Spray freezing into liquid nitrogen for highly stable protein nanostructured microparticles, Eur. J. Pharm. Biopharm. 58 (2004) 529–537.

[21] Z. Yu, K.P. Johnston, R.O. Williams III, Spray freezing into liquid versus spray-freeze drying: Influence of atomization on protein aggregation and biological activity, Eur. J. Pharm. Sci. 27 (2006) 9–18.

[22] M.C. Heller, J.F. Carpenter, T.W. Randolph, Protein formulation and lyophilization cycle design: prevention of damage due to freeze-concentration induced phase separation, Biotechnol. Bioeng. 63 (1999) 166–174.

[23] H. Sitte, L. Edelmann, K. Neumann, Cryofixation without pretreatment at ambient pressure, in: R.A. Steinbrecht, K. Zierold (Eds.), Cryotechniques in Biological Electron Microscopy, Springer-Verlag, Berlin, 1987, pp. 87–113.

[24] M.J. Costello, J.M. Corless, The direct measurement of temperature changes within freeze-fracture specimens during rapid quenching in liquid coolants, J. Microsc. 112 (1978) 17–37.
[25] H. Gieseler, PhD Thesis, University of Erlangen-Nuremburg, 2004.
[26] M.K. Barron, T.J. Young, K.P. Johnston, R.O. Williams III, Investigation of processing parameters of spray freezing into liquid to prepare polyethylene glycol polymeric particles for drug delivery, AAPS Pharm. Sci. Tech. 4 (2003) 1–13.
[27] S. Mawson, S. Kanakia, K.P. Johnston, Coaxial nozzle for control of particle morphology in precipitation with a compressed fluid antisolvent, J. Appl. Polym. Sci. 64 (1997) 2105–2118.
[28] J.D. Engstrom, D.T. Simpson, C. Cloonan, E. Lai, R.O. Williams III, G.B. Kitto, K.P. Johnston, Stable high surface area lactate dehydrogenase particles produced by spray freezing into liquid nitrogen (submitted for publication).
[29] S. Brunauer, P.H. Emmett, E. Teller, Adsorption of gases in multimolecular layers, J. Am. Chem. Soc. 60 (1938) 309–319.
[30] A.A. Elkordy, R.T. Forbes, B.W. Barry, Integrity of crystalline lysozyme exceeds that of a spray-dried form, Int. J. Pharm. 247 (2002) 79–90.
[31] Y.-H. Liao, M.B. Brown, A. Quader, G.P. Martin, Protective mechanism of stabilizing excipients against dehydration in the freeze-drying of proteins, Pharm. Res. 19 (2002) 1854–1861.
[32] A.H. Lefebvre, Atomization and Sprays, Hemisphere Publishing Corporation, New York, 1989, pp. 27–78.
[33] R.D. Reitz, F.V. Bracco, Mechanisms of breakup of round liquid jets, in: N.P. Cheremisinoff (Ed.), Encyclopedia of Fluid Mechanics, Gulf Publishing Co., Book Division, Houston, 1986, pp. 233–249.
[34] B.J. Meister, G.F. Scheele, Drop formation from cylindrical jets in immiscible liquid systems, AIChE J. 15 (1969) 700–706.
[35] D.J. Dixon, K.P. Johnston, R.A. Bodmeier, Polymeric materials formed by precipitation with a compressed fluid antisolvent, AIChE J. 39 (1993) 127–139.
[36] C.S. Lengsfeld, J.P. Delplanque, V.H. Barocas, T.W. Randolph, Mechanism governing microparticle morphology during precipitation by a compressed antisolvent: atomization vs. nucleation and growth, J. Phys. Chem. B 104 (2000) 2725–2735.
[37] E. Badens, O. Boutin, G. Charbit, Laminar jet dispersion and jet atomization in pressurized carbon dioxide, J. Supercrit. Fluids 36 (2005) 81–90.
[38] N. Czerwonatis, R. Eggers, Disintegration of liquid jets and drop drag coefficients in pressurized nitrogen and carbon dioxide, Chem. Eng. Tech. 24 (2001) 619–624.
[39] J. Baldyga, M. Henczka, B.Y. Shekunov, Fluid dynamics, mass transfer, and particle formation in supercritical fluids, Drugs Pharm. Sci. 138 (2004) 91–157.
[40] F. Kreith, M.S. Bohn, Principles of Heat Transfer, Harper and Row, Publishers, Inc., New York, 1986, pp. 360–363.
[41] F.P. Incropera, D.P. DeWitt, Fundamentals of Heat and Mass Transfer, John Wiley and Sons, New York, 2002, pp. 243–254.
[42] J.A.N. Zasadzinski, A new heat transfer model to predict cooling rates for rapid freezing fixation, J. Microsc. 150 (1988) 137–149.
[43] S.M. Bailey, J.A.N. Zasadzinski, Validation of convection-limited cooling of samples for freeze-fracture electron microscopy, J. Microsc. 163 (1991) 307–320.
[44] H.Y. Elder, C.C. Gray, A.G. Jardine, J.N. Chapman, W.H. Biddlecombe, Optimum conditions for cryoquenching of small tissue blocks in liquid coolants, J. Microsc. 126 (1982) 45–61.
[45] F. Franks, Biophysics and Biochemistry at Low Temperatures, Cambridge University Press, New York, 1985, pp. 21–187.
[46] C.A. Angell, Liquid fragility and the glass transition in water and aqueous solutions, Chem. Rev. 102 (2002) 2627–2649.
[47] A.P. MacKenzie, Non-equilibrium freezing behavior of aqueous systems, Philos. Trans. R. Soc. Lond. B: Biol. Sci. 278 (1977) 167–189.
[48] S.L. Nail, S. Jiang, S. Chongprasert, S.A. Knopp, Fundamentals of freeze-drying, in: S.L. Nail, M.J. Akers (Eds.), Pharmaceutical Biotechnology. 14. Development and Manufacture of Protein Pharmaceuticals, Kluwer Academic/Plenum Publishers, New York, 2002, pp. 281–360.
[49] M.C. Heller, J.F. Carpenter, T.W. Randolph, Application of a thermodynamic model to the prediction of phase separations in freeze-concentrated formulations for protein lyophilization, Arch. Biochem. Biophys. 363 (1999) 191–201.
[50] N.H. Fletcher, Structural aspects of the ice–water system, Rep. Prog. Phys. 34 (1971) 913–994.
[51] E. Mayer, P. Brueggeller, Vitrification of pure liquid water by high pressure jet freezing, Nature 298 (1982) 715–718.
[52] J.F. Carpenter, K.-i. Izutsu, T.W. Randolph, Freezing- and drying-induced perturbations of protein structure and mechanisms of protein protection by stabilizing additives, in: L. Rey, J.C. May (Eds.), Drugs and the Pharmaceutical Sciences. 137. Freeze-Drying/Lyophilization of Pharmaceutical and Biological Products, Marcel Dekker Inc., New York, 2004, pp. 147–186.
[53] M.T. Cicerone, C.L. Soles, Fast dynamics and stabilization of proteins: binary glasses of trehalose and glycerol, Biophys. J. 86 (2004) 3836–3845.